HILLOCK INTERACTIONS DURING CALCITE GROWTH OBSERVED USING *IN SITU* ATOMIC FORCE MICROSCOPY

A Thesis

Presented to the Faculty of the Graduate School

of Cornell University

In Partial Fulfillment of the Requirements for the Degree of

Master of Science

by

Jeremy Brett Gershonowitz

August 2019

ABSTRACT

Calcite, the most thermodynamically stable form of $CaCO_3$, is a common biomineral found in marine organisms such as mollusks and sea urchins. The calcite structures found in these organisms often display non-equilibrium morphologies and increased fracture toughness compared to geologic calcite. It has been shown that the rhombohedral morphology of calcite single crystals grown via spiral growth is reflected in the rhombohedral shape of growth hillocks at the atomic scale. The underlying cause of this similarity is poorly understood. To better understand this morphological link, we present here an *in-situ* Atomic Force Microscopy study of interactions between neighboring hillocks in pure calcite, and in calcite grown in the presence of glycine. We discovered that in pure calcite, neighboring hillocks can interact in exactly three geometries. Each geometry has a characteristic morphology and effect on the growth of the crystal. We show that the addition of glycine alters these characteristics due to changes in the shape of the hillock and the kinetics at the step edge. Lastly, we present observational evidence of hillock overgrowth, a hypothesis of the factors that cause overgrowth, and a discussion of the implications that hillock overgrowth has on the bulk scale morphology of the crystal. The results presented in this thesis narrow the research gap of the phenomenological link between the atomic and bulk scale morphologies of calcite crystals and may inform future studies that aim to narrow this research gap as well.

BIOGRAPHICAL SKETCH

Jeremy Gershonowitz was born in 1996 in New York City. He developed an appreciation for science and technology and Hunter College High School, which led to his desire to study engineering in college. Jeremy attended Cornell University for his undergraduate studies, where he majored in Materials Science and Engineering. Classes in materials chemistry and mechanical properties of materials cemented his desire to better understand the fundamental properties of materials.

Jeremy joined Professor Lara Estroff's research group in January of 2017. Under the training of Dr. Coit Hendley IV, Jeremy began his project of characterizing hillock interactions in pure calcite using *in-situ* Atomic Force Microscopy. Jeremy's work on this project led to the submission of his senior thesis in May 2018.

For his graduate studies, Jeremy continued working on the same project in Professor Estroff's research group at Cornell University. During his graduate studies, his project expanded to include characterization of calcite growth in the presence of glycine as well as the characterization of hillock overgrowth in calcite. After graduation, he will begin full-time employment as an R&D Chemist at Parker Chomerics.

ACKNOWLEDGMENTS

I would like to thank all of those who have helped me achieve my goal of completing my Master of Science degree in Materials Science and Engineering. First and foremost, I would like to thank Professor Estroff, my major committee chair member for her guidance and encouragement in the 2.5 years that I have been a part of her research group. I could not have asked for a more helpful and understanding mentor to guide me through my undergraduate and graduate studies. I would also like to thank Professor Shefford Baker, my minor committee chair member, for the insight and advice he has given me on this project. I would like to thank Dr. Coit Hendley IV for patiently training me in the difficult technique of *in situ* Atomic Force Microscopy and for being a great reservoir of information on the scientific literature. I would like to thank Hengyu Zhou, Amnon Ortoll-Bloch, and Konrad Hedderick, all of whom contributed data that made the completion of this project possible. I would like to thank the rest of the members of the Estroff group for their support and feedback. Lastly, I would like to thank my friends and family for their support, love, and encouragement.

TABLE OF CONTENTS

LIST OF FIGURES

Chapter 1.

Introduction and Background

1.1 Spiral Growth in Calcite

Many marine organisms use the abundance of ions in seawater to grow crystalline structures from calcite ($CaCO_3$) that comprise the structural components of their bodies [1]. These crystals, grown from solution, often have increased hardness [2] and fracture toughness [3], and non-equilibrium morphologies [4] compared to their geologic equivalents. In an effort to understand the origin of the improved mechanical properties and unusual morphologies, the field of biomineralization was born and has led to the extensive study of the solution growth of crystals. Crystal growth from solution requires a solution that is supersaturated with respect to the ions that compose the crystal. Supersaturation is defined by the equation $\ln(\sigma) = \frac{\Delta\mu}{k_bT} = \ln(\frac{a}{K_{sp}})$, where $\Delta\mu$ is the change in chemical potential per molecule, k_b is Boltzmann's constant, T is absolute temperature, and a and K_{sp} are the actual and equilibrium activity products of the ions in solution. At supersaturations just above equilibrium ($1 < \sigma \lesssim 1.4$), crystals grow by the spiral growth mechanism [5].

Following the classic terrace-step-kink crystal growth model, spiral growth occurs when ions from the solution attach at the intersection of screw dislocations with the surface (Fig 1.1). Ions attach along this intersection, in the form of a step, and propagate in the perpendicular direction to the step edge (Figure 1.2). As this step propagates, a new segment is created following the crystallographic orientation of the crystal and the handedness of the screw dislocation. This segment is relatively immobile until it becomes longer than the average spacing between kink nucleation sites. Once this segment exceeds this length, known as the critical length, L_c, it will

begin to propagate in the direction perpendicular to the step edge. The result of this mechanism is the attachment of ions in a faceted spiral which grows vertically from the surface. The resultant formation is known as a dislocation hillock or a growth hillock. Growth hillocks are characterized by their shape, critical length, step height, step propagation velocity, and terrace width. Terrace width is defined as the length between two adjacent steps of the same orientation, or in other words, how far a step has progressed in the time it has taken the spiral to make one full rotation. Hillock shape and step height are functions of the crystal structure. Critical length, step velocity, and terrace width are functions of both the crystal structure and the supersaturation of the solution.

Although spiral growth was first theorized to occur by Burton, Frank, and Cabrera (BCF) in 1951 [6,7], hillocks were only able to be visualized in 3D with the use of Atomic Force Microscopy (AFM) in late 1990's [8]. *In-situ* AFM experiments are done by imaging the surface of a crystal while a supersatured solution is flowed through a fluid cell containing the crystal (Figure 1.3).

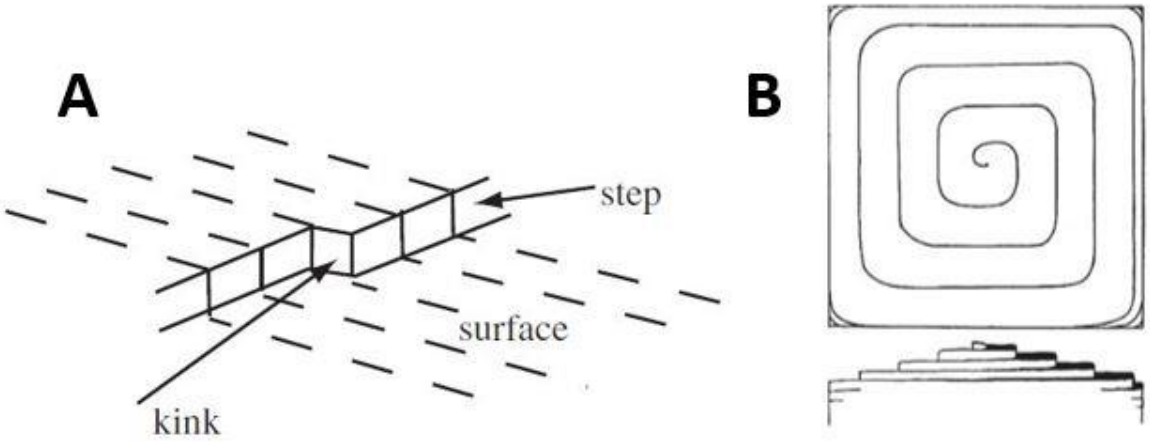

Figure 1.1. (A) Schematic of the classical Terrace(Surface)-Step-Kink model describing different attachment sites on the crystal surface. The energy cost of the adsorption of a solute molecule is lowest at kink sites and highest at terraces. Using this model, Burton, Cabrera, and Frank theorized the formation of growth hillocks from the intersection of screw dislocations with the crystal surface. (B) A schematic of a hillock as seen from above the surface (top) and parallel to the surface (bottom). The hillock in the schematic is generated from a right handed screw dislocation and has made five complete turns, generating five atomic layers [6].

Spiral growth in crystals such as Calcite ($CaCO_3$) [5, 9-12], Calcium Oxalate Monohydrate ($CaC_2O_4 \cdot H_2O$) [13-15], Brushite ($CaHPO_4 \cdot 2H_2O$) [12,19-20], and Potassium Dihydrogen Phosphate (KH_2PO_4) [16-18] have since been extensively studied using *in-situ* AFM.

On its most easily cleaved plane, $\{10\bar{1}4\}$, calcite forms growth hillocks such that steps propagate from the dislocation source in four directions, creating four faces (Figure 1.2). Two of

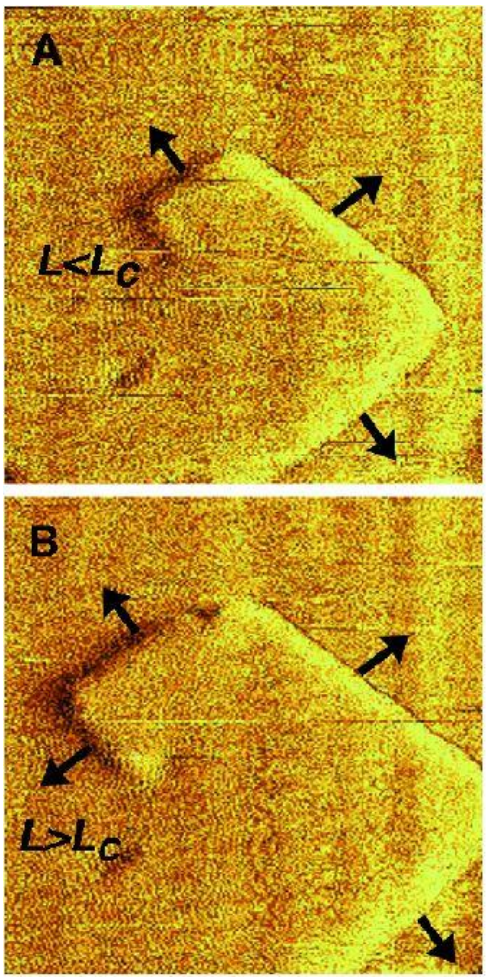

Figure 1.2. (A) *in-situ* AFM image of a hillock in calcite nucleated on the intersection of a right handed screw dislocation with the surface. The smallest step of atoms has not yet reached the critical length L_c and continues to grow in the direction parallel to the step edge. (B) The step from (A) has exceeded the critical length and begins to propagate away from the dislocation source perpendicular to the step edge. The formation of a new step perpendicular to this step begins and becomes a new turn in the spiral. From Teng, H.H., Dove, P.M., Orme, C.A., De Yoreo, J.J. Thermodynamics of Calcite Growth: Baseline for Understanding Biomineral Formation. *Science*. **282**, 724-727 (1998).. Reprinted with permission from AAAS [8].

these faces propagate approximately perpendicular to the $[\bar{4}41]$ direction and two approximately perpendicular to the $[48\bar{1}]$ direction. By nature of the rhombohedral unit cell of calcite, one of each of these faces forms an acute (-) angle with the surface at the step edge; The other two form an obtuse (+) angle. These two angles are supplementary. Each step has a height of 3.1Å.

Step propagation in calcite is rate limited by the generation of kink sites on the step edge [21]. Crystal growth in the classic terrace-step-kink model assumes a high density of kink sites along step edges due to minimization of the Gibbs free energy of the crystal-solution system. Under

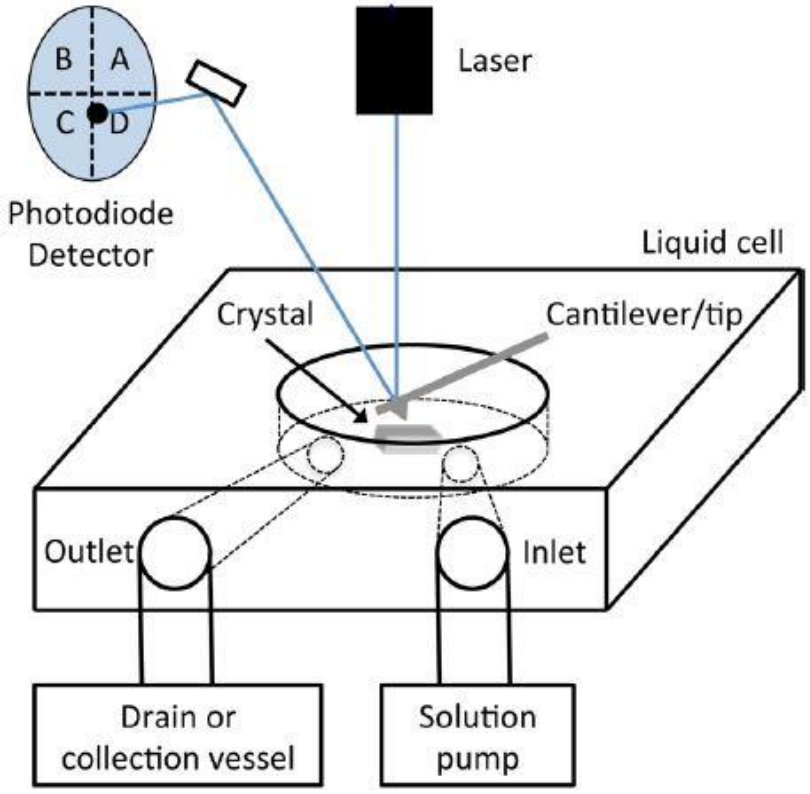

Figure 1.3. Schematic of the *in situ* AFM experimental setup. The fluid cell contains a chamber in which the sample is placed. There is an inlet and outlet connected to the chamber that solution can flow through. An AFM tip mounted on a cantilever is placed in the chamber and a laser is reflected off of the cantilever into a photodiode. Changes in height of the sample deflect that cantilever, which in turn deflects the position of the laser on the photodiode. The changes in position of the laser on the photodiode are translated into a topographic map of the surface. Reprinted (Adapted or Reprinted in part) with permission from Poloni, L.N., Zhong, X., Ward, M.D., Mandal, T. Best Practices for Real-Time in Situ Atomic Force and Chemical Force Microscopy of Crystals. *Chem. Mater.* **29**, 331-345 (2017). Copyright 2017 American Chemical Society [38].

this assumption, step growth is rate limited by the attachment and detachment of solute particles to kink sites on the step. Using *in-situ* AFM, it has been shown that calcite does not follow the classic model as kink site density and atomic fluctuation along the step edge is relatively low. The low rate of kink site generation replaces the attachment of solute particles to the step as the rate limiting factor in step growth in calcite.

1.2 Morphological Effects of Molecular Scale Additives in Calcite

Thermodynamic and kinetic Wulff plots have been used since the early 1900's to understand and predict bulk scale crystal growth and shape [22]. Wulff plots predict the equilibrium shape of a crystal based on Gibbs' equilibrium condition for faceted crystals by stating that the perpendicular distance from a crystal face to the origin of the crystal is proportional to the surface free energy per unit area [23]. Wulff plots are an exceptional tool for predicting and understanding bulk crystal growth. It is clear, however, that morphology control in biominerals occurs at the atomic scale and therefore requires a deeper look at the origins of crystal morphology as a function of additives.

Despite the faceted nature of single crystals, biominerals can be found in a variety of shapes. The variance in shape is due in part to the significant control organisms have over the biomineral growth process. One way in which organisms may control the shape of biominerals is by the inclusion of molecular scale additives [24]. Many molecular scale additives have been shown to modify the bulk scale and atomic scale morphology of calcite [25-28]. Marine organisms have access to seawater ions, peptides, polysaccharides, and proteins during the biomineralization process. For example, calcite in mollusk shells contains inclusions of magnesium ions, highly

acidic proteins, and chitin, a polysaccharide [29]. Spiral growth of calcite in the presence of each of these categories of additives has been studied extensively [10,30-32].

Orme et al. were the first to show that there exists a phenomenological link between the atomic scale and bulk scale morphology of calcite with and without the presence of additives [4, 25]. Specifically, they showed the shape of growth hillocks in calcite reflects the shape of bulk scale crystals grown with the same additives (Figure 1.4). For example, the acute faces of calcite hillocks become rounded when grown in the presence of D-Asp and L-Asp. Bulk crystals of calcite grown in the presence of L-Asp and D-Asp showed the same rounded morphology. Additionally, hillocks with D-Asp have mirrored symmetry to those of L-Asp. The same is true of the bulk crystals. It can be concluded that shape control of bulk scale single crystals must be controlled at the atomic level. When considering a single hillock growing on an otherwise atomically flat calcite surface, the link between the atomic and bulk scale is not difficult to rationalize. However, many hillocks populate the surface of a growing calcite crystal [33]. Without a proper understanding of how hillocks interact with each other, the phenomenological link is not

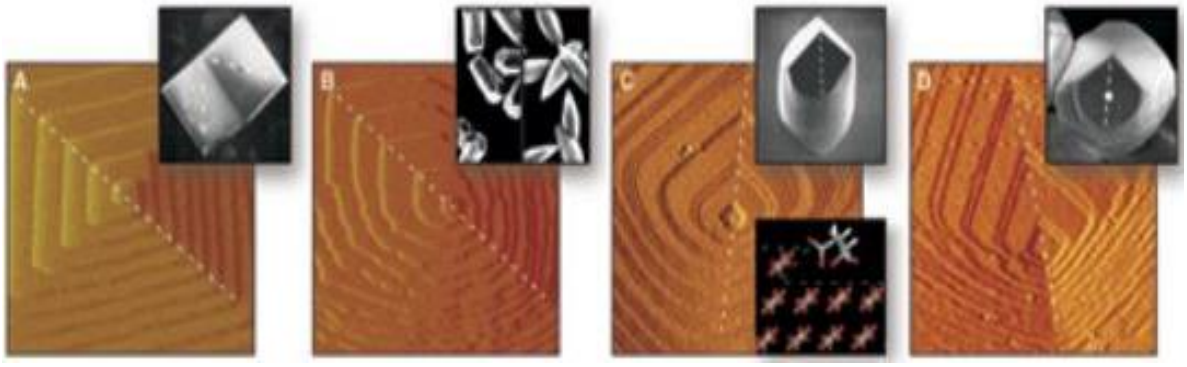

Figure 1.4. The bulk scale shape of calcite crystals grown via spiral growth is reflected in the atomic morphology of the growth hillocks. From left to right, AFM images of hillocks are shown in conjunction with SEM images of bulk calcite crystals grown in the presence of no additives, Mg^{2+}, D-Asp, and the small protein AP8. The shape of each hillock matches the shape of each SEM image of the bulk crystal, showing that macroscale shape is influenced by the atomic scale morphology From De Yoreo, J.J., Dove, P.M. Shaping Crystals with Biomolecules. *Science*. **306**, 1301-1302 (2004). Reprinted with permission from AAAS [4].

easily explained. This thesis aims to characterize the ways in which hillocks interact in calcite so that we may better understand this phenomenological link.

1.3 Structure-Function Effects of Molecular Scale Additives in Calcite

In addition to their morphological effects on single crystals of calcite, molecular scale additives have been shown to change the mechanical properties of single crystals of calcite. The mechanical effects of additives such as magnesium ions [34-36], and biomacromolecules such as amino acids [2,37] have been studied in calcite. These additives have been shown to increase the hardness [2] and fracture toughness [3] of calcite single crystals. Additive rich calcite composes structural components in marine organisms such as mollusks and sea urchins. The study of the structure-function effects of additives in calcite has led to the conclusion that magnesium and amino acids are incorporated into the lattice. However, using *in-situ* AFM, Orme et al. concluded that amino acids are not incorporated into the lattice because the step velocities on the calcite surface do not decrease with the presence of amino acids [25]. The discrepancy between bulk scale *ex-situ* calcite growth studies of the mechanical properties of additives and nanoscale *in-situ* growth studies of morphological effects of additives remains unexplained. By understanding the growth mechanisms between the nanoscale and the bulk scale, we may be able to resolve this discrepancy. This thesis aims to better understand growth in this intermediate scale by studying the interactions between hillocks in calcite.

1.4 References

1. Nudelman, F., Sommerdijk, N.A.J.M. Biomineralization as an Inspiration for Materials Chemistry. *Angew Chem. Int. Ed*. **51**, 6581-6596 (2012).

2. Kim, Y.Y., Carloni, J.D. Demarchi, B. Sparks, D. Reid, D. Kunitake, M.E., Tang, C.C., Duer, M.J., Freeman, C.L., Pokroy, B., Penkman, K., Harding, J., Estroff, L.A., Baker, S.P., Meldrum, F.C. Tuning Hardness in Calcite by Incorporation of Amino Acids. *Nature Mater.* **15**, 903-910 (2016).

3. Polischuk, I., Bracha, A.A., Bloch, L. et al. Coherently aligned nanoparticles within a biogenic single crystal: A biological prestressing strategy. *Science*. **358**, 1295-1298 (2017).

4. De Yoreo, J.J., Dove, P.M. Shaping Crystals with Biomolecules. *Science*. **306**, 1301-1302 (2004).

5. De Yoreo, J.J., Vekilov, P.G. Principles of Nucleation and Growth. *Reviews in Mineraleology & Geochemistry*. **54**, 57-93 (2003).

6. Burton, W.K., Cabrera, N., Frank, F.C. THE GROWTH OF CRYSTALS AND THE EQUILIBRIUM STRUCTURE OF THEIR SURFACES. *Proc. R. Soc. Lond. A*. **243**, 299-358 (1951).

7. Woodruff, D.P. How does your crystal grow? A commentary on Burton, Cabrera, and Frank (1951) 'The growth of crystals and the equilibrium structure of their surfaces'. *Phil. Trans. R. Soc. A.* **373**, (2015).

8. Teng, H.H., Dove, P.M., Orme, C.A., De Yoreo, J.J. Thermodynamics of Calcite Growth: Baseline for Understanding Biomineral Formation. *Science*. **282**, 724-727 (1998).

9. Davis, K.J., Dove, P.M., De Yoreo, J.J. The Role of Mg^{2+} as an Impurity in Calcite Growth. *Science*. **290**, 1134-1137 (2000).

10. Qiu, S.R., Orme, C.A. Dynamics of Biomineral Formation at the Near-Molecular Level. *Chemical Reviews.* ***108***, 4784-4819 (2008).

11. Teng, H.H., Dove, P.M., De Yoreo, J.J. Kinetics of calcite growth: Surface processes and relationships to macroscopic rate laws. *Geochim. Cosmochim. Acta*. **64**, 2255-2266 (2000).

12. Orme, C.A., Giocondi, J.L. The use of scanning probe microscopy to investigate crystal-fluid interfaces. *Perspectives on Inorganic, Organic, and Biological Crystal Growth: From Fundamentals to Applications (ISSCG-13)*. **916**, 342-+ (2007).

13. Qiu, S.R., Wierzbicki, A., Orme, C.A. et al. Molecular modulation of calcium oxalate crystallization of osteopontin and citrate. *P. Natl. Acad. Sci. USA*. **101**, 1811-1815 (2003).

14. Chernov, A.A., Petrova, E., Rashkovich, L.N. Dependence of the CaOx and MgOx growth rate on solution stoichiometry. *Crystal Growth*. **289**, 245-254 (2006).

15. Rashkovich, L.N., Petrova, E.V. Chernevich, T.G. et al. Non-Kossel crystals: Calcium and magnesium oxalates. *Crystallography Reports*. **50**, S78-S81 (2005).

16. Giocondi, J.L., El-Dasher, B.S., Nancollas, G.H., Orme, C.A. Molecular mechanisms of crystallization impacting calcium phosphate cements. *Phil. Trans. R. Soc. A.* **368**, 1937-1961 (2010).

17. Tang, R., Nancollas, G.H., Giocondi, J.L., Hoyer, J.R., Orme, C.A. Dual roles of brushite crystals in calcium oxalate crystallization provide physiochemical mechanisms underlying renal stone formation. *Kidney International*. **70**, 71-78 (2006).

18. Land, T.A., De Yoreo, J.J., Martin, T.L., Palmore, G.T. A comparison of growth Hillock structure and step dynamics on KDP {100} and {101} surfaces using force microscopy. *Crystallography Reports*. **44**, 655-666 (1999).

19. De Yoreo, J.J., Land, T.A., Rashkovich, L.N. et al. The effect of dislocation cores on growth hillock vicinality and normal growth rates of KDP {101} surfaces. *Crystal Growth*. **182**, 442-460 (1997).

20. De Yoreo, J.J., Orme, C.A., Land, T.A. Using atomic force microscopy to investigate solution crystal growth. *ISSCG-11*. 361-380 (2001).

21. De Yoreo, J.J., Zepeda-Ruiz, L.A., Friddle, R.W. et al. Rethinking Classical Crystal Growth Models through Molecular Scale Insights: Consequences of Kink-Limited Kinetics. *Crystal Growth & Design*. **9**, 5135-5144 (2009).

22. Wulff, G. On the question of speed of growth and dissolution of crystal surfaces. *Krystallogr.* **34**, 449-530 (1901).

23. Gadewar, S.B., Doherty, M.F. A dynamic model for evolution of crystal shape. *Crystal Growth*. **267**, 239-250 (2004).

24. Weber, E. Pokroy, B. Intracrystalline inclusions within single crystalline hosts: from biomineralization to bio-inspired crystal growth. *Cryst. Eng. Comm.* **17,** 5873-5883 (2015).

25. Orme, C.A., Noy, A., Wierzbicki, A. et al. Formation of chiral morphologies through selective binding of amino acids to calcite surface steps. *Nature.* **411,** 775-779 (2001).

26. Davis, K. J., Dove, P.M., DeYoreo, J.J. The Role of Mg^{2+} as an Impurity in Calcite Growth. *American Mineralogist.* **89,** 714-720 (2004).

27. Davis, K. J., Dove, P.M., Wasylenki, L.E. Morphological Consequences of Differential Mg^{2+} Incorporation at Structurally Distinct Steps on Calcite. *Science.* **290,** 1134-1137 (2000).

28. Wasylenski, L.E., Dove, P.M., Wilson, D.S., et al. Nanoscale effects of strontium on calcite growth: An in situ AFM study in the absence of vital effects. *Geochimica et Cosmochimica Acta.* **69,** 3017-3027 (2005).

29. Li, H., Xin, H.L., Kunitake, M.E., et al. Calcite Prisms from Mollusk Shells (*Atrina Rigida*): Swiss-cheese-like Organic-Inorganic Single-crystal Composites. *Adv. Fun. Mater.* **21,** 2028-2034 (2011).

30. Metzler, R. A., Tribello, G. A., Parrinello, M. & Gilbert, P. Asprich peptides are occluded in calcite and permanently disorder biomineral crystals. *J. Am. Chem. Soc*. **132,** 11585-11591 (2010).

31. Albeck, S., Aizenberg, J., Addadi, L., Weiner, S. Interactions of various skeletal intracrystalline components with calcite crystals. *J. Am. Chem. Soc*. **115,** 11691-11697 (1993).

32. Aizenberg, J., Hanson, J., Koetzle, T. F.,Weiner, S. & Addadi, L. Control of macromolecule distribution within synthetic and biogenic single calcite crystals. *J. Am. Chem. Soc.* **119,** 881-886 (1997).

33. Chernov, A.A., Rashkovich, L.N., Mkrtchan, A.A. SOLUTION GROWTH KINETICS AND MECHANISM: PRISMATIC FACE OF ADP. *Crystal Growth*. **74,** 101-112 (1986)

34. Kunitake, M. E., Baker, S. P. & Estroff, L. A. The effect of magnesium substitution on the hardness of synthetic and biogenic calcite. *MRS Commun.* **2,** 113-116 (2012).

35. Kunitake, M.E., Mangano, L.M., Peloquin, J.M., Baker, S.P., Estroff, L.A. Evaluation of strengthening mechanisms in calcite single crystals from mollusk shells. *Acta Biomaterialia*. **9,** 5353-5359 (2013)

36. Ma, Y., Aichmayer, B., Paris, O., The grinding tip of the sea urchin tooth exhibits exquisite control over calcite crystal orientation and Mg distribution. *P. Natl. Acad. Sci. USA*. **106,** 6048-6053 (2009).

37. Borukhin, S. et al. Screening the incorporation of amino acids into an inorganic crystalline host: the case of calcite. *Adv. Funct. Mater.* **22,** 4216-4224 (2012).

38. Poloni, L.N., Zhong, X., Ward, M.D., Mandal, T. Best Practices for Real-Time in Situ Atomic Force and Chemical Force Microscopy of Crystals. *Chem. Mater.* **29**, 331-345 (2017).

Chapter 2. Hillock Interactions During Calcite Growth Observed Using *In Situ* Atomic Force Microscopy

2.1. Introduction and Experimental Design

2.1.1 Introduction

Calcite, the most thermodynamically stable form of $CaCO_3$, is a common biomineral found in marine organisms such as mollusks and sea urchins. These organisms exercise precise control over the growth of calcite, with molecular scale additives such as Mg^{2+}, amino acids, and proteins [1] found in biogenic single crystals. These additives have been shown to alter the atomic and bulk scale morphology of calcite [2], leading to non-equilibrium morphologies and increased fracture toughness and hardness compared to the geologic equivalent [2-9].

Biogenic calcite single crystals are grown from solution in seawater, which is supersatured with respect to calcium and carbonate ions [8]. To better understand the effect of additives on the mechanical properties and the morphology of biogenic calcite, solution growth of single crystalline calcite in the presence of molecular scale additives has been studied extensively [1,10-27]. Most studies have focused on solution growth in the low supersaturation regime where the spiral growth mechanism dominates. Specifically, these studies have characterized the growth of individual growth hillocks. Here, we present a characterization of the interactions between neighboring hillocks in calcite grown via spiral growth.

It has been shown that the rhombohedral bulk scale morphology of calcite single crystals grown via spiral growth is reflected in the rhombohedral shape of their growth hillocks [24]. This correlation has been shown to exist with and without the presence of molecular scale additives. This phenomenological link shows that the bulk scale morphology of single crystals of calcite is

controlled by the atomic level growth mechanism and kinetics. When considering a single hillock growing on an otherwise atomically flat surface, the phenomenological link is easily understood. However, many hillocks populate the surface during growth [28], making the phenomenological link difficult to rationalize. To understand the connection between the atomic scale and the bulk scale, it is necessary to understand how individual hillocks interact with each other. We define an interaction between two hillocks as the collision of steps propagating from two distinct dislocation sources.

Interactions between hillocks were first discussed by Burton, Cabrera, and Frank (BCF) in their 1951 paper theorizing the existence of spiral growth [29]. In this paper, BCF discuss hillock growth nucleated from multiple dislocation sources and how these hillocks might interact. BCF state that if two screw dislocation sources of the same handedness are within 2π critical lengths of each other, a hillock with twice the step density will form as a result. They state that this hillock formation will have a higher activity than a normal hillock and will dominate the surface. If the dislocation sources are of opposite handedness and within 2π critical lengths of each other, BCF state that no growth will occur in this region. When the dislocation sources are greater than 2π critical lengths apart, BCF state that if they are of the same handedness, they will produce a hillock with the same activity as a single source hillock, but the morphology will be elongated. If the dislocation sources are of opposite handedness, they state that instead of a spiral, the sources will generate concentric loops that propagate outwards again with the same activity as a single source hillock.

In experimental work, Chernov et al. presented evidence of hillocks overgrowing neighboring hillocks in Ammonium Dihydrogen Phosphate (ADP) as a response to changing supersaturation using Laser Michelson interferometry [29]. De Yoreo et al. stated that hillocks with

high step density originating from multiple Burgers vector dislocation sources will overgrow hillocks with lower step density [14]. It has been shown that in brushite ($CaHPO_4 \cdot 2H_2O$), the corners formed from collisions between steps propagating in different directions have a high density of kink sites and facilitate higher step velocities in this region [19].

2.1.2 Experimental Design

The aim of this study is to characterize hillock interactions in calcite. Characterization of hillock interactions in calcite requires an experimental technique that has atomic level resolution in the z-axis, nanometer resolution in the xy plane, is effective in solution, and captures data on a timescale compatible with growth rates during spiral growth. The most suitable technique for these requirements is *in-situ* Atomic Force Microscopy (AFM) [8]. AFM performs at the necessary resolution and can be done in fluid. We carefully selected a supersaturation at which the step velocities were such that the AFM could properly track their progression, but not so slow that the AFM could not resolve the terraces between steps. To maximize the rate of data collection, we chose to work in contact mode rather that tapping mode. By using *in situ* AFM, we were able to clearly visualize the calcite surface as it grew.

2.2 Experimental

2.2.1 *In Situ* Atomic Force Microscopy

Samples were cleaved from large bulk crystals of geologic calcite (Iceland Spar, Ward's Scientific). Samples were approximately 1.5cm x 1.5cm x 0.2 cm. The samples were then mounted on 1.5 cm AFM stubs and N_2 gas was flowed over the sample to remove any loosely attached particles from the surface. 100 mL of 0.18mM $CaCO_3$ solution was prepared from

$CaCl_2$ and $NaHCO_3$ salts (Sigma Aldrich). 0.394 mmol of NaCl salt (Sigma Aldrich) was added to the solution to increase ionic strength to 0.00502 from 0.00108 and deter formation of CO_2 from CO_3^{2-} ions. $CaCO_3$ solution was transferred into syringes in increments of 25 mL. The syringes were sealed with parafilm to deter diffusion of CO_2 into the solution. The calcite sample was placed in a Bruker MultiMode 8 AFM such that the obtuse/obtuse corner of the sample was in the back left of the stage. The AFM tip was loaded into a Bruker MTFML fluid cell and enclosed in an elastomeric O-Ring which sealed a chamber between the tip and the sample for fluid to flow through. Bruker SNL-10 and DNP-S10 tips were used. The $CaCO_3$ solution was flowed through the fluid cell at a rate of 0.3 mL/min. A portion of the surface with a height variation of less than 20nm was located and the tip was then engaged in contact mode. The field of view was set to 20μm x 20μm and the scan rate was set to 3.00 Hz at 256 samples per line. Scans were done at a 315° scan angle to clearly image all four hillock faces. The scan angle is defined as the angle between the direction perpendicular to the edge of the cantilever the tip is mounted on, and the horizontal component of the scanning direction. The tip was scanned laterally across the surface until an area with multiple stable hillocks was located within the field of view. New solution was used every 20 minutes to deter CO_2 diffusion into the system. In experiments with glycine, after the location of two stable hillocks, 100 mL of $CaCO_3$ solution was prepared with the addition of 0.18mM of glycine (Sigma Aldrich, 99% purity). This solution was drawn in 25mL increments into syringes and used in the same manner as the pure $CaCO_3$ solution.

2.3 Results and Discussion

2.3.1 Proposed Hillock Interactions in Pure Calcite

Consider a hillock on the $\{10\bar{1}4\}$ calcite surface oriented such that the c-glide plane bisects the hillock vertically, with the obtuse faces of the hillock above the acute faces of the hillock. In this orientation, obtuse steps propagate diagonally upwards and acute steps propagate diagonally downwards. The propagation directions of these steps are similar to, but not exactly the same as the directions perpendicular to the crystal facets due to the difference in mobility of kink site diffusion along the step edge in acute and obtuse steps. We have chosen to represent these directions as a, a', b, and b' (Fig 2.1). Consider a second hillock, located at any point in the $\{10\bar{1}4\}$ plane except at the location of the first hillock. Hillocks grown on the same facet of a single crystal must have the same orientation. Despite the infinite possible locations of the second hillock in the plane, it can be shown that there are only three distinct ways in which two calcite hillocks can interact. These three hillock interaction types depend on two factors: the step edge geometry and the angle between the step velocity vectors of the colliding steps (Fig 2.1).

We define a Type I hillock interaction as the collision of steps propagating from two dislocation sources such that their step velocities are antiparallel (Figure 2.1A). Type I interactions occur when steps travelling in either the a and a' directions, or the b and b' directions collide. In this alignment, the colliding steps have opposite step edge geometries, that is, one is acute, and one is obtuse. These step edge geometries are due to the rhombohedral lattice of calcite and hold true for any rhombohedral system. The result of this alignment is the head on collision of acute steps with obtuse steps. Because the acute and obtuse angles are supplementary, the result is an annihilation of the steps and the completion of a terrace.

Completed terraces provide a surface for the steps above the annihilated ones to propagate on and eventually annihilate as well. The global result of the Type I hillock interaction is the vertical growth of the surface at the valley between the two hillocks. Assuming terrace width is

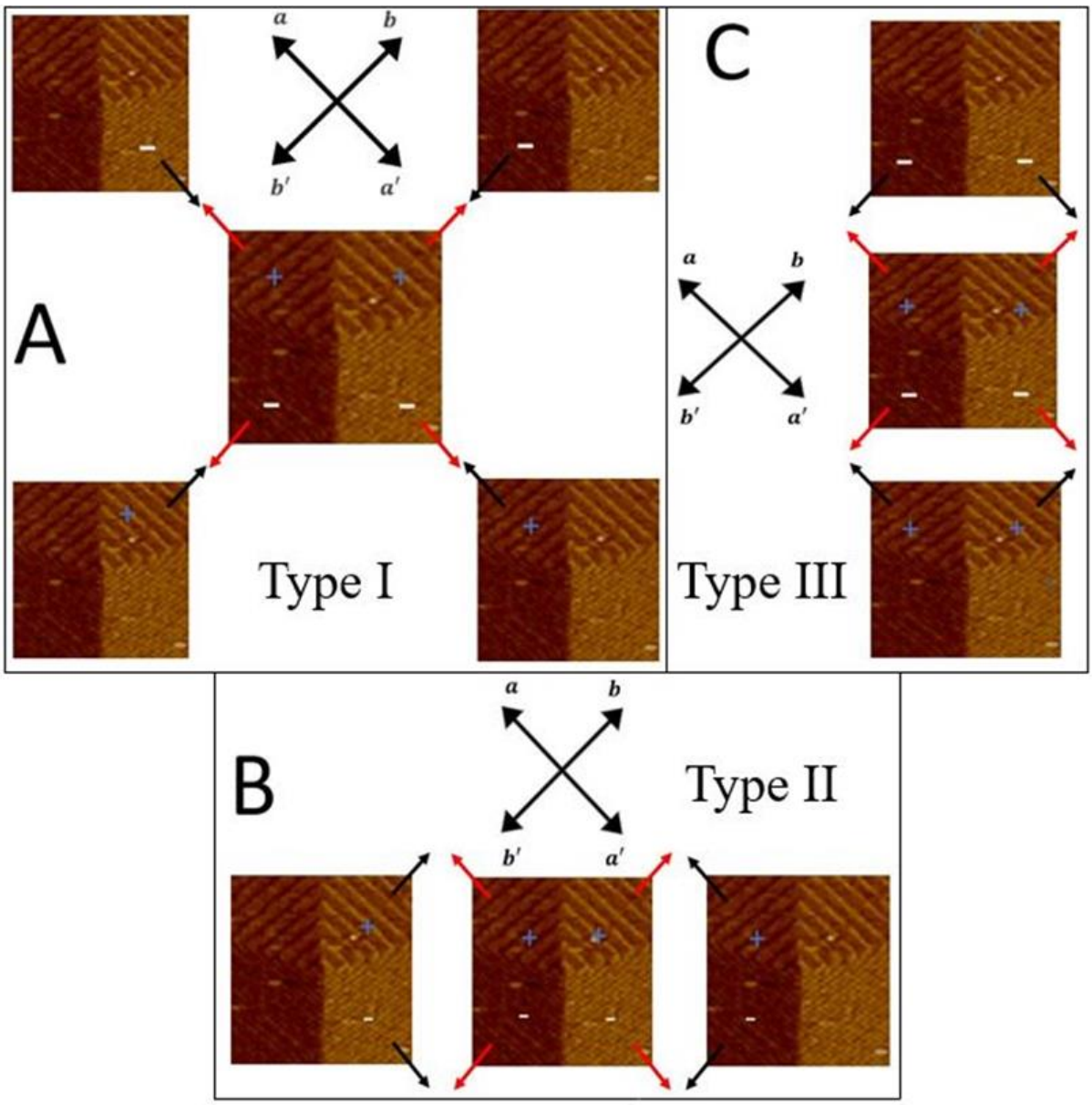

Figure 2.1. The interactions between two hillocks are dependent on their relative positioning. There are three distinct types of hillock interactions. (A) Type I hillock interactions occur when steps propagating in either the a and a' directions, or the b and b' directions collide. (B) Type II hillock interactions occur when steps propagating in either the a and b directions, or the a' and b' directions collide. (C) Type III hillock interactions occur when steps propagating in either the a and b' directions, or the a' and b directions collide. The hillocks in this schematic are oriented such that the obtuse faces (+) are above the acute faces (-).

constant along the entire hillock, the vertical growth rate in this valley is equal to the vertical growth rate at the dislocation source. This relationship must be true because each step propagates one terrace width for every complete turn of the spiral at the dislocation source. When two steps collide and annihilate, the steps above them will be separated by a distance of two terrace widths. These steps will annihilate once they have each propagated one terrace width, the time it takes for one turn of the spiral. Since the surface grows by the height of one unit cell after one turn of the spiral as well as after the annihilation of two steps, it can be concluded that the vertical growth rates at the dislocation source and the valley are equal.

We define Type II and Type III hillock interactions as the collision of steps propagating from two dislocation sources such that their step velocities not antiparallel (Figure 2.1B). The differentiation between these two hillock interaction types comes from the step edge geometries of the interacting faces. In Type II Hillock interactions, the interacting faces have similar step edge geometries, that is, both acute or both obtuse. Type II interactions occur when steps travelling in either the a and b directions, or the a' and b' directions collide. Unlike the head-on collisions in Type I interactions, Type II collisions occur at a single point that joins the two steps at an obtuse angle. A new kink site is generated at the point of collision. There is no potential barrier for the formation of kink sites at the point of collision [6]. Whereas the addition of a growth unit to kink sites on the step edge has no net effect on the kink site density in the crystal, the addition of a growth unit to the kink site generated in Type II interactions increases the kink site density. Due to the increased kink site density originating at the step collision point, growth in this region occurs more rapidly than at the step edge. The rapid growth in this area causes a rounding effect on the colliding steps as the area between them is filled by growth units. Similar

step rounding due to increased kink site density has been observed in etch pits of calcite at the intersection of perpendicular steps [30].

We define Type III hillock interactions as the collision of steps from two dislocation sources such that the step velocities not antiparallel, and the step edge geometries of the interacting steps are different (Figure 2.1C). Type III interactions occur when steps travelling in either the a and b' directions, or the a' and b directions collide. Although this hillock interaction produces a new kink site as in Type II interactions, the step rounding phenomenon does not occur due to the differing adsorption rates of ions in solution to acute and obtuse steps. It has been shown that the rate of ion adsorption, and therefore the step velocity of acute and obtuse steps, depends individually on the activity ratio of the Ca^{2+} and CO_3^{2-} ions in solution [31,32]. When Ca^{2+}:CO_3^{2-} is near unity or above, the affinity for adsorption on the obtuse steps is much larger than that of the acute step. At low Ca^{2+}:CO_3^{2-}, growth on the acute steps are favored. For large enough differences in adsorption energies on the acute and obtuse steps, the preference for a certain step edge geometry outweighs the preference for growth in the region of the new kink site. The steps will then advance in the direction they normally would, with the step velocity of the preferred step edge geometry being larger. In the case where the activity ratio yields no preference for step edge geometry, similar rounding behavior to Type II hillock interactions can be expected, although this condition has not been tested.

2.3.2 Experimental Verification of Hillock Interactions

To obtain experimental evidence for the three types of hillock interactions proposed in Fig. 2.1, we performed *in-situ* AFM. Figure 2.2 shows sequential AFM images of a Type I hillock interaction. The colliding steps have antiparallel step velocities and have opposing step

edge geometry. 28 minutes into the experiment, steps from the two hillocks propagate on a terrace towards each other. At 32 minutes, the first steps collide. These steps annihilate, forming a terrace for the next steps to propagate on. For the remainder of the experiment, the annihilation of steps between the two hillocks continues. Analysis of the AFM data shows that the terrace width and relative height between the two hillocks remains constant for the duration of the experiment.

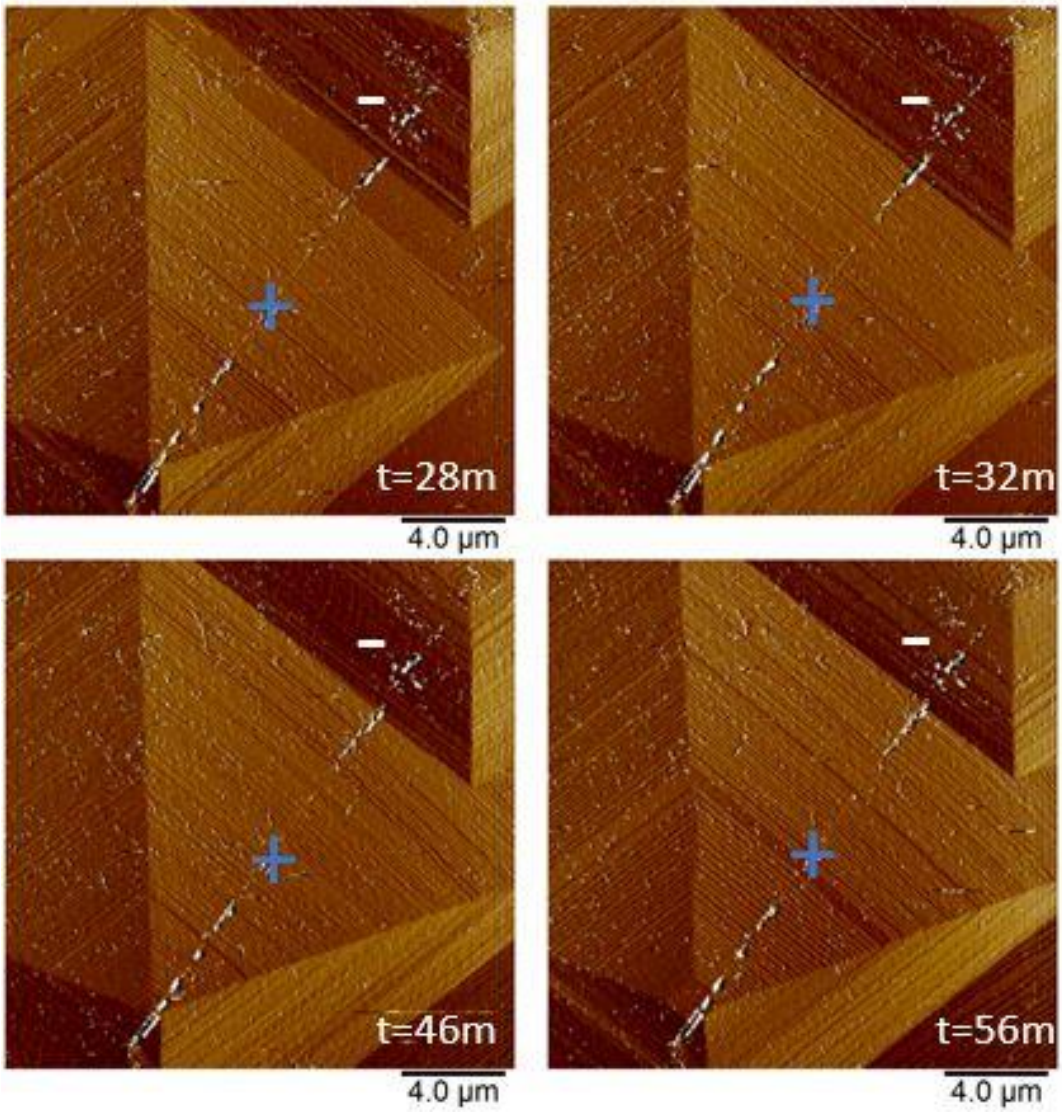

Figure 2.2. AFM images of Type I interaction between two hillocks with the relevant step edge geometries labeled. Supersaturation was set to $\sigma = 1.14$ with flow rate of 0.3 mL/min. Time relative to the beginning of the experiment.

Figure 2.3 shows sequential AFM images of a Type II hillock interaction. Steps from the two hillocks collide in two areas. In both areas, the propagating steps collide at an angle and have similar step edge geometries. It can be seen 13 minutes into the experiment that the steps between the two hillocks both on the acute and the obtuse faces have collided and become rounded. Between 21 and 56 minutes, the bottom hillock begins to dominate the top hillock on the obtuse-obtuse interaction site. The interaction in this area shifts from completely Type II to mostly Type I with Type II interactions occurring at the top of the steps of the upper hillock.

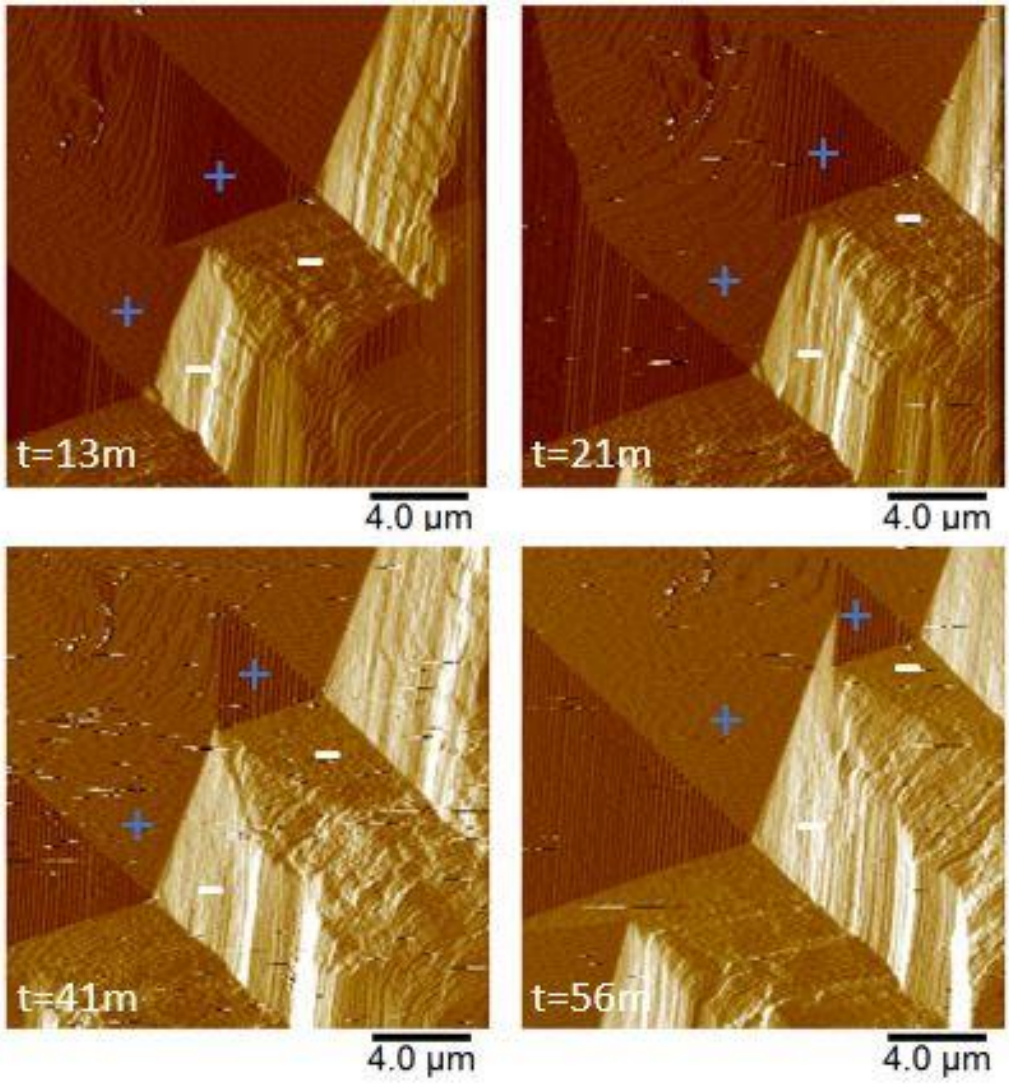

Figure 2.3: AFM images of a Type II interaction between two hillocks with relevant step edge geometries labeled. Supersaturation was set to σ=1.14 with flow rate of 0.3 mL/min. Time relative to the beginning of the experiment.

Steps from a third hillock interact with the lower hillock at 56 minutes. These steps are acute and propagating at an angle to the acute steps of the lower hillock, so this interaction is Type II as well. The characteristic step rounding is once again present.

Figure 2.4 shows sequential AFM images of a Type III hillock interaction. Steps from the two hillocks collide in three areas. In the outer areas, the steps collide at an angle, and have opposing step edge geometries. This interaction is Type III. In between these two areas, there is a

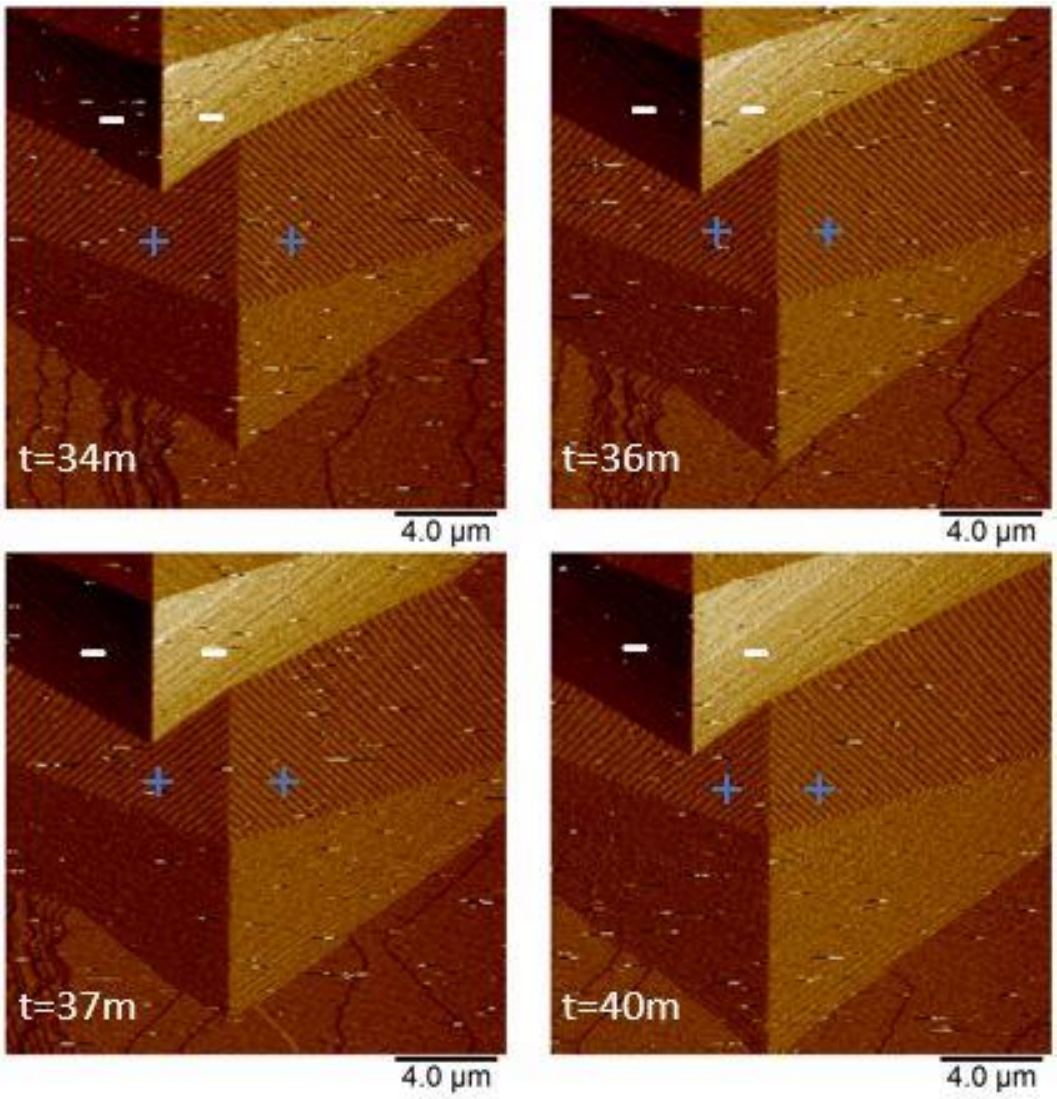

Figure 2.4. AFM images of a Type III interaction between two hillocks with relevant step edge geometries labeled. Supersaturation was set to σ=1.14 with flow rate of 0.3 mL/min. Supersaturation was set to σ=1.14 with flow rate of 0.3 mL/min. Time relative to the beginning of the experiment.

small length of Type I interaction where the colliding steps have antiparallel step velocities and opposing step edge geometries. Because of the opposing step edge geometries, no step rounding is present in the areas with Type III interactions. The activity ratio Ca^{2+}:CO_3^{2-} was equal to one in this experiment, so growth on the obtuse steps was heavily favored. The preference for growth on the obtuse steps can be seen by the rapid advancement of obtuse steps onto the terrace in the upper right hand corner.

2.3.3 Proposed Hillock Interactions in the Presence of Glycine

When grown in the presence of glycine, the acute-acute corner and the acute-obtuse corners of calcite hillocks become rounded while the obtuse-obtuse corner and the middle of the steps are unaffected. This change in morphology occurs due to the change in step edge free energy when glycine interacts with the corners of the hillock [24]. Based on *in-situ* AFM experiments, it has been suggested that glycine does not incorporate into the calcite lattice, but rather changes the morphology by acting as a surfactant. In other work based on *ex-situ* bulk growth, glycine is shown to incorporate, even with no bulk morphology change observed [33]. The change in hillock morphology due to glycine affects how calcite hillocks interact with each other.

In pure calcite, acute steps propagate only in the a' and b' directions. The rounding of the acute corners in the presence of glycine generates step propagation with all directions encompassed between a' and b'. The continuous nature of the step propagation directions on the acute faces causes a shift from Type I to Type III hillock interaction character when the obtuse steps of one hillock interact across the acute-acute corner of another hillock (Figure 2.5). The regions with Type I and Type III character behave as they would in pure calcite. The growth on

the obtuse steps in the area of the acute-acute corner is still faster and growth units fill in near the collision point as they would in Type III hillock interactions in pure calcite.

Figure 2.5 shows sequential AFM images of Type I and Type III hillock interactions with glycine present. 76 minutes into the experiment, steps from a hillock nucleated out of the field of view to the left collide with the steps from the hillock nucleated in the upper right of the image.

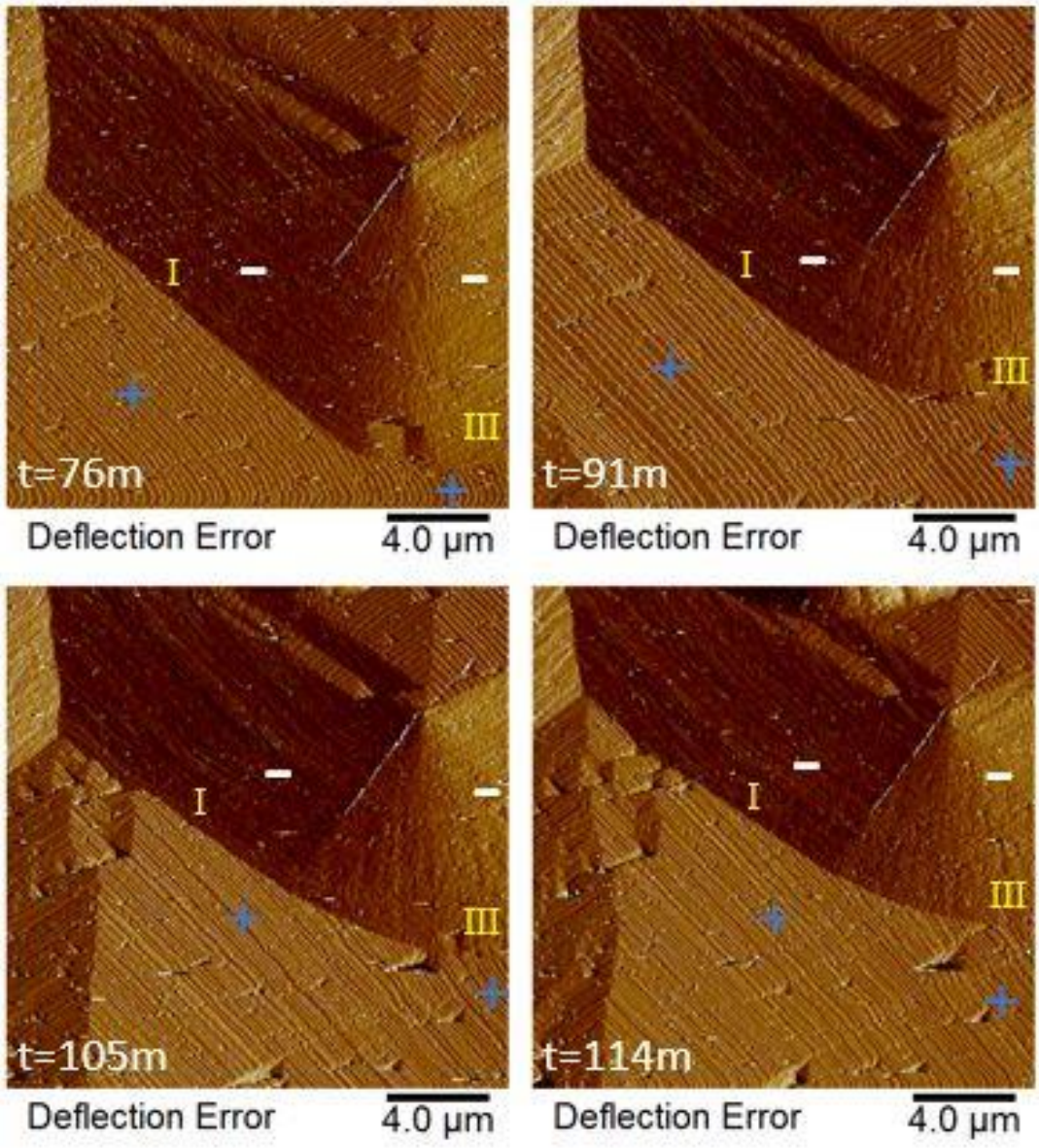

Figure 2.5. AFM images of Type I and Type III hillock interactions in the presence of glycine. Type I and Type III interactions are labeled. Supersaturation was set to σ=1.14 with flow rate of 0.3 mL/min. [Gly]=0.18mM. Time relative to the beginning of the experiment.

The effect of glycine is apparent from the roundedness of the acute-acute corner of the upper right hillock. The interaction transitions from Type I to Type III character moving left to right across the intersection of the two hillocks. At 105 minutes, multiple small hillocks have nucleated on surface defects, which can be seen in the previous images.

In Type II hillock interactions in pure calcite, the step rounding effect is the same for steps that are both acute and steps that are both obtuse. Both interactions generate energetically "free" kink sites at the collision point and rapid growth at the collision point leads to step rounding. With the addition of glycine, acute Type II interactions cannot be treated the same as obtuse Type II interactions since glycine molecules preferentially adsorb to and change the kinetics of the acute steps. For Type II interactions in calcite grown in the presence of glycine, we have observed that step rounding does not occur (Figure 2.6). The addition of glycine to a pure calcite system reverses the step rounding previously present on the acute steps. Because the acute steps in the presence of glycine become rounded, they must have an abundance of kink sites. In pure calcite, step growth is rate limited by the sparse generation of kink sites on the step edge [21], however, in the presence of glycine, the rate limiting step becomes the attachment and detachment of growth units at kink sites along the step. The lack of dependence on the generation of kink sites makes the impact of an energetically free kink site not nearly as important in the presence of glycine as it was in pure calcite. Because the newly generated kink site does not have a significant impact on the rate of growth at the collision point between the two steps in a Type II interaction, the step rounding morphology is not incentivized, and therefore does not occur.

Figure 2.6 shows sequential AFM images of a Type II hillock interaction in pure calcite and in the presence of glycine. 47 minutes into the experiment, two hillocks in a pure calcite

system have nucleated. All three hillock types are visible between these two hillocks (Type II, Type I, and Type II moving down and left along the intersection line of the hillocks.) The circled area shows the step rounding effect that is characteristic of Type II interactions in pure calcite. The same step rounding is present and more pronounced at 59 minutes. At 67 minutes, glycine is added to the system, which can be seen by the rounding of the acute corners of the hillocks. The

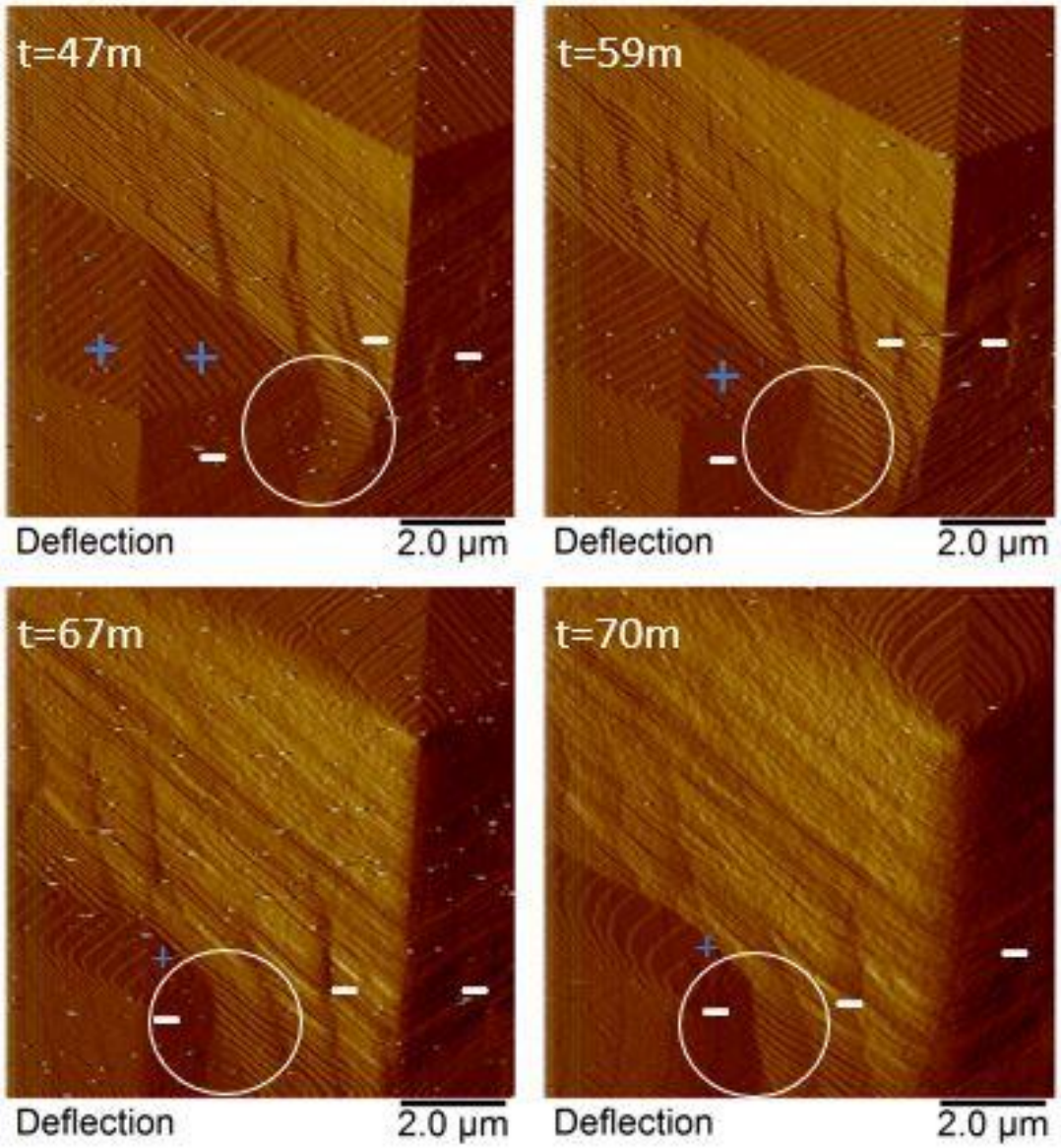

Figure 2.6. AFM images of Type II hillock interaction without (top) and with (bottom) the presence of glycine. Supersaturation was set to σ=1.14 with flow rate of 0.3 mL/min. [Gly]=0.18mM, added at t=67 minutes. Time relative to the beginning of the experiment. Circled areas highlight Type II interactions.

step rounding effect is immediately less pronounced and is completely gone by 70 minutes once glycine has been fully mixed into the fluid cell. The collision points between the steps at 70 minutes curves inward to a sharp point due to the roundedness of the obtuse-acute corner of the lower left hillock.

2.3.4 Hillock Overgrowth

Hillock overgrowth occurs when the steps propagating from one hillock advance towards the dislocation source of the other hillock. Sometimes, a complete overgrowth occurs when the propagating steps from one hillock eclipse the dislocation source of another hillock. Understanding the causes and kinetics of hillock overgrowth may lead to a better understanding of the link between the atomic and macroscopic scale morphologies of calcite single crystals. The kinetic factors that allow hillock overgrowth are not completely understood; However, it can be shown that certain hillock features invariably enable overgrowth.

A hillock with high step density will overgrow a hillock with low step density (Figure 2.7). In a Type I Hillock interaction between a high and low step density hillocks, steps from the higher step density hillock will annihilate progressively further from the dislocation source. This advancement leads to the partial or complete overgrowth of the low step density hillock. This method of overgrowth was theorized by BCF and has been reasserted by other studies since [5,12,27]. Step density is a function of supersaturation, and since all hillocks on the same surface are exposed to the same conditions, it would not be expected that hillock overgrowth can occur. However, hillocks formed from multiple dislocations sources or multiple Burgers vector dislocation sources have increased step density. Regardless of its origin, it is clear that increased step density enables hillock overgrowth.

Figure 2.7 shows two examples of hillock overgrowth from increased step density. In Fig. 2.7A, the upper hillock has a higher step density than the lower. In Fig. 2.7B, after 6 minutes, the upper hillock has advanced on the lower, shown by the decreasing length of the white arrow. Figures 2.7C and 2.7D show a different experiment in which two hillocks have nucleated on the surface. The hillock nucleated to the left of the field of view has twice the step density of the

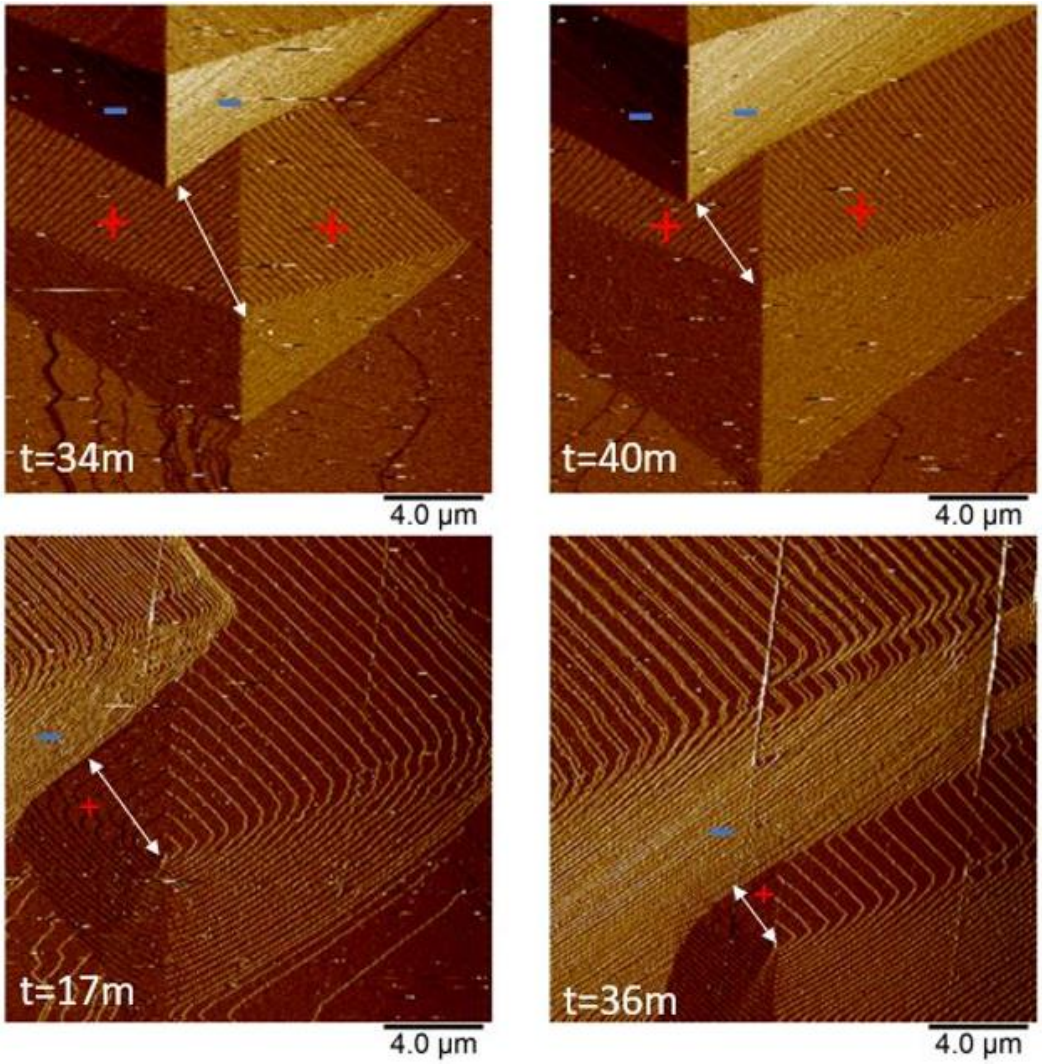

Figure 2.7. Sequential AFM images of two different experiments showing hillock overgrowth due to differences in step density. A,B) Hillock overgrowth shown by the decreasing length of the white arrow. C,D) Hillock overgrowth shown by the decreasing length of the white arrow. The hillock with larger step density has nucleated left of the field of view. Supersaturation was set to σ=1.14 with flow rate of 0.3 mL/min. Time relative to the beginning of the experiment.

hillock nucleated in the image. The higher step density hillock advances on the lower, shown by the decreasing length of the white arrow. Had these experiments continued for a longer duration, the low step density hillocks would eventually have been overgrown by the higher step density hillocks.

Our present hypothesis on what controls the phenomenological link between hillock and bulk scale morphology is that regions of high step density originating from hillocks dominate the surface and eventually form the edges of the bulk crystal. We have observed increased step density in hillocks nucleated from a single source, as well as in hillocks nucleated from groupings of nearby sources. We believe that aggregates of dislocation sources and hillocks may create large regions of high step density, which would dominate the surface and form the crystal. To support this hypothesis, more AFM data must be collected on high step density hillocks and hillock aggregates with different relative positionings of the dislocation sources.

2.4 Conclusion

The ways in which hillocks can interact in calcite are finite. We characterized the ways in which hillocks can interact on the calcite surface during spiral growth both in pure calcite, and calcite grown in the presence of glycine. In pure calcite, we defined Type I hillock interactions as the collision of steps propagating in parallel directions. These steps were shown to annihilate, leading to the stable vertical growth of the surface. We defined Type II hillock interactions as the collision of steps propagating in perpendicular directions that have similar step edge geometries. Type II hillock interactions were shown to have a characteristic step rounding due to the rapid generation of kink sites at the point of collision. Type III hillock interactions were defined as the collision of steps propagating in perpendicular directions that have opposite step edge

geometries. It was shown that these collisions did not have any step rounding due to the difference in step edge energies of the acute and obtuse steps in calcite at the solution parameters we used. Instead, it was shown that the obtuse steps dominated growth in the area into which steps from both hillocks were propagating.

The addition of glycine to the system has little impact on Type I and Type III hillock interactions. The only noticeable difference is the smooth transition from Type I to Type III character due to the roundedness of the acute-acute corner. The addition of glycine reverses the step rounding effect on the acute steps seen in Type II interactions in pure calcite. This morphological change arises from the fact that the curved region of the acute steps has an abundance of kink sites. The abundance of kink sites changes the rate limiting factor in step growth from kink site generation to rate of attachment and detachment of growth units from solution. The lack of dependence on kink site generation makes the newly generated kink site at the collision point negligible to the overall growth rate in the region, and so, the step rounding morphology seen in pure calcite does not occur in the presence of glycine.

We showed observational evidence of hillock overgrowth due to increased step density and activity of certain hillocks. Hillock overgrowth is fundamental to understanding the phenomenological link between the morphology of hillocks and the bulk crystal. The data collected on high activity hillocks, in addition to the characterization of hillock interactions, lays the groundwork for understanding the mechanism behind this phenomenological link.

2.5 References

1. Li, H., Xin, H.L., Kunitake, M.E., et al. Calcite Prisms from Mollusk Shells (*Atrina Rigida*): Swiss-cheese-like Organic-Inorganic Single-crystal Composites. *Adv. Fun. Mater.* **21,** 2028-2034 (2011).

2. De Yoreo, J.J., Dove, P.M. Shaping Crystals with Biomolecules. *Science*. **306**, 1301-1302 (2004).

3. Kunitake, M. E., Baker, S. P. & Estroff, L. A. The effect of magnesium substitution on the hardness of synthetic and biogenic calcite. *MRS Commun.* **2,** 113-116 (2012).

4. Kunitake, M.E., Mangano, L.M., Peloquin, J.M., Baker, S.P., Estroff, L.A. Evaluation of strengthening mechanisms in calcite single crystals from mollusk shells. *Acta Biomaterialia*. **9,** 5353-5359 (2013)

5. Ma, Y., Aichmayer, B., Paris, O., The grinding tip of the sea urchin tooth exhibits exquisite control over calcite crystal orientation and Mg distribution. *P. Natl. Acad. Sci. USA*. **106,** 6048-6053 (2009).

6. Borukhin, S. et al. Screening the incorporation of amino acids into an inorganic crystalline host: the case of calcite. *Adv. Funct. Mater.* **22,** 4216-4224 (2012).

7. Burton, W.K., Cabrera, N., Frank, F.C. THE GROWTH OF CRYSTAS AND THE EQUILIBRIUM STRUCTURE OF THEIR SURFACES. *Proc. R. Soc. Lond. A*. **243**, 299-358 (1951)

8. Qiu, S.R., Orme, C.A. Dynamics of Biomineral Formation at the Near-Molecular Level. *Chemical Reviews.* ***108***, 4784-4819 (2008).

9. Polischuk, I., Bracha, A.A., Bloch, L. et al. Coherently aligned nanoparticles within a biogenic single crystal: A biological prestressing strategy. *Science*. **358**, 1295-1298 (2017).

10. De Yoreo, J.J., Vekilov, P.G. Principles of Nucleation and Growth. *Reviews in Mineraleology & Geochemistry*. **54**, 57-93 (2003).

11. Teng, H.H., Dove, P.M., Orme, C.A., De Yoreo, J.J. Thermodynamics of Calcite Growth: Baseline for Understanding Biomineral Formation. *Science*. **282**, 724-727 (1998).

12. K.J., Dove, P.M., De Yoreo, J.J. The Role of Mg^{2+} as an Impurity in Calcite Growth. *Science*. **290**, 1134-1137 (2000).

13. Teng, H.H., Dove, P.M., De Yoreo, J.J. Kinetics of calcite growth: Surface processes and relationships to macroscopic rate laws. *Geochim. Cosmochim. Acta*. **64**, 2255-2266 (2000).

14. Qiu, S.R., Wierzbicki, A., Orme, C.A. et al. Molecular modulation of calcium oxalate crystallization of osteopontin and citrate. *P. Natl. Acad. Sci. USA*. **101**, 1811-1815 (2003).

15. Chernov, A.A., Petrova, E., Rashkovich, L.N. Dependence of the CaOx and MgOx growth rate on solution stoichiometry. *Crystal Growth*. **289**, 245-254 (2006).

16. Rashkovich, L.N., Petrova, E.V. Chernevich, T.G. et al. Non-Kossel crystals: Calcium and magnesium oxalates. *Crystallography Reports*. **50**, S78-S81 (2005)

17. Giocondi, J.L., El-Dasher, B.S., Nancollas, G.H., Orme, C.A. Molecular mechanisms of crystallization impacting calcium phosphate cements. *Phil. Trans. R. Soc. A.* **368**, 1937-1961 (2010)

18. Tang, R., Nancollas, G.H., Giocondi, J.L., Hoyer, J.R., Orme, C.A. Dual roles of brushite crystals in calcium oxalate crystallization provide physiochemical mechanisms underlying renal stone formation. *Kidney International*. **70**, 71-78 (2006)

19. Orme, C.A., Giocondi, J.L. The use of scanning probe microscopy to investigate crystal-fluid interfaces. *Perspectives on Inorganic, Organic, and Biological Crystal Growth: From Fundamentals to Applications (ISSCG-13)*. **916**, 342-+ (2007)

20. Land, T.A., De Yoreo, J.J., Martin, T.L., Palmore, G.T. A comparison of growth Hillock structure and step dynamics on KDP {100} and {101} surfaces using force microscopy. *Crystallography Reports*. **44**, 655-666 (1999)

21. De Yoreo, J.J., Land, T.A., Rashkovich, L.N. et al. The effect of dislocation cores on growth hillock vicinality and normal growth rates of KDP {101} surfaces. *Crystal Growth*. **182**, 442-460 (1997)

22. De Yoreo, J.J., Orme, C.A., Land, T.A. Using atomic force microscopy to investigate solution crystal growth. *ISSCG-11*. 361-380 (2001)

23. De Yoreo, J.J., Zepeda-Ruiz, L.A., Friddle, R.W. et al. Rethinking Classical Crystal Growth Models through Molecular Scale Insights: Consequences of Kink-Limited Kinetics. *Crystal Growth & Design*. **9**, 5135-5144 (2009).

24. Orme, C.A., Noy, A., Wierzbicki, A. et al. Formation of chiral morphologies through selective binding of amino acids to calcite surface steps. *Nature.* **411,** 775-779 (2001).

25. Davis, K. J., Dove, P.M., DeYoreo, J.J. The Role of Mg^{2+} as an Impurity in Calcite Growth. *American Mineralogist.* **89,** 714-720 (2004).

26. Davis, K. J., Dove, P.M., Wasylenki, L.E. Morphological Consequences of Differential Mg^{2+} Incorporation at Structurally Distinct Steps on Calcite. *Science.* **290,** 1134-1137 (2000).

27. Wasylenski, L.E., Dove, P.M., Wilson, D.S., et al. Nanoscale effects of strontium on calcite growth: An in situ AFM study in the absence of vital effects. *Geochim. Cosmochim. Acta.* **69,** 3017-3027 (2005).

28. Chernov, A.A., Rashkovich, L.N., Mkrtchan, A.A. SOLUTION GROWTH KINETICS AND MECHANISM: PRISMATIC FACE OF ADP. *Crystal Growth*. **74**, 101-112 (1986).

29. Burton, W.K., Cabrera, N., Frank, F.C. THE GROWTH OF CRYSTALS AND THE EQUILIBRIUM STRUCTURE OF THEIR SURFACES. *Proc. R. Soc. Lond. A*. **243**, 299-358 (1951).

30. Jordan, G., Rammensee, W. Dissolution rates of calcite (1014) obtained by scanning force microscopy: Microtopography-based dissolution kinetics on surfaces with anisotropic step velocities. *Geochim. Cosmochim. Acta.* **62**, 941-947 (1998).

31. Stack, A.G., Grantham, M.C. Growth Rate of Calcite Steps As a Function of Aqueous Calcium-to-Carbonate Ratio: Independent Attachment and Detachment of Calcium and Carbonate Ions. *Crystal Growth & Design*. **10**, 1409-1413 (2010).

32. Larsen, K., Bechgaard, K., Stipp, S.L.S. The effect of the Ca^{2+} to CO_3^{2-} activity ratio on spiral growth at the calcite {1014} surface. *Geochim. Cosmochim. Acta*. **74**, 2099-2109 (2009).

33. Kim, Y.Y., Carloni, J.D. Demarchi, B. Sparks, D. Reid, D. Kunitake, M.E., Tang, C.C., Duer, M.J., Freeman, C.L., Pokroy, B., Penkman, K., Harding, J., Estroff, L.A., Baker, S.P., Meldrum, F.C. Tuning Hardness in Calcite by Incorporation of Amino Acids. *Nature Mater.* **15**, 903-910 (2016).

Chapter 3.

Conclusion and Future Work

This thesis aimed to characterize hillock interaction using *in situ* AFM as a first step towards understanding the phenomenological link between the atomic and bulk scale shape of calcite crystals. I characterized these interactions in pure calcite growth and in calcite growth in the presence of glycine. I found that in pure calcite, exactly three types of hillock interactions are possible. I defined these hillock interactions on the basis of their step propagation directions and step edge geometries. Each hillock interaction was characterized in terms of its morphological effect on the surface both in pure calcite growth and in calcite growth in the presence of glycine. I also provided AFM data showing hillock overgrowth by high activity hillocks. This data was used to provide a hypothesis of a mechanism that could explain the link between the morphologies of the growth hillocks at the nanoscale and the whole crystal at the bulk scale.

The *in* situ AFM experiments were only done with pure calcite and calcite in the presence of glycine; However, these same experiments can be done with other additives. In the future, characterization of calcite hillock interactions in the presence of other amino acids, proteins, and nanoparticles could help to understand the details of calcite morphology at the atomic and bulk scale. Glycine has been shown to act as a surfactant when modifying the growth of calcite hillocks, but other additives have been shown to alter hillock growth via step-pinning, incorporation, kink blocking, and acting as a surfactant [1]. Using additives that interact with calcite hillocks by different mechanisms may provide further insight into hillock-hillock interactions.

The *in situ* AFM experiments done in this thesis were all run with identical solution parameters. Varying the concentrations of Ca^{2+} and CO_3^{2-} would help to further understand the

surface kinetics involved with hillock interactions and would also reinforce the statements made in this thesis. This thesis predicts that at low Ca^{2+}:CO_3^{2-} activity ratios, Type III hillock interactions in pure calcite should look the same except that the acute steps should be favored. This thesis also predicts that at the Ca^{2+}:CO_3^{2-} activity ratio such that growth velocity on each step is identical, Type III hillock interactions should behave like Type II hillock interactions and step rounding should occur. These predictions, while logically sound, were not corroborated with experimental evidence. Studying calcite growth in these activity ratio regimes would provide evidence for these predictions and would also help to further our understanding of hillock interactions in calcite.

Hillock overgrowth is integral to understanding the phenomenological link between the bulk scale morphology and the shape of growth hillocks in calcite single crystals. In this thesis, I presented a brief review of the literature on hillock overgrowth, including a discussion of the double source hillocks theorized by BCF [2]. Future work should use *in situ* AFM to observe the behavior of double source hillocks. All of the types of double source hillocks theorized by BCF should be observed. The relative positioning of the sources may have an impact on the growth of the hillock. We have collected AFM data showing a clear example of a hillock with two opposite handed sources which are more than half a critical length apart (Figure 3.1). An example of this kind of hillock source exists in the literature, though the paper does not discuss it [3]. Both of these examples behave as BCF predicts. Observing a double source hillock with the sources within half a critical length of each other may be difficult with the current resolution limitations of *in situ* AFM in fluid.

Beyond *in situ* AFM experiments, it will be very useful to run kinetic Monte Carlo (KMC) simulations of the calcite surface. One of the limiting factors of AFM is the field of view. For the experiments in this thesis, the field of view was set to 20 µm x 20 µm. Any field of view much larger will require a long time to produce a single image, which is not ideal for observing crystal growth. KMC simulations can be done over a much larger field of view as they are only limited by the capabilities of the software. Kinetic Monte Carlo will allow us to simulate nucleation and growth of many hillocks based on predetermined surface conditions on a larger field of view. Molecular Dynamic and KMC simulations have been used to study calcite growth [4,5]. We hope to use these techniques in the future to observe long range interactions that arise from hillock interactions, for example, the long range effects of high step density hillocks. This technique will also be helpful in studying the long range behavior of hillock aggregates.

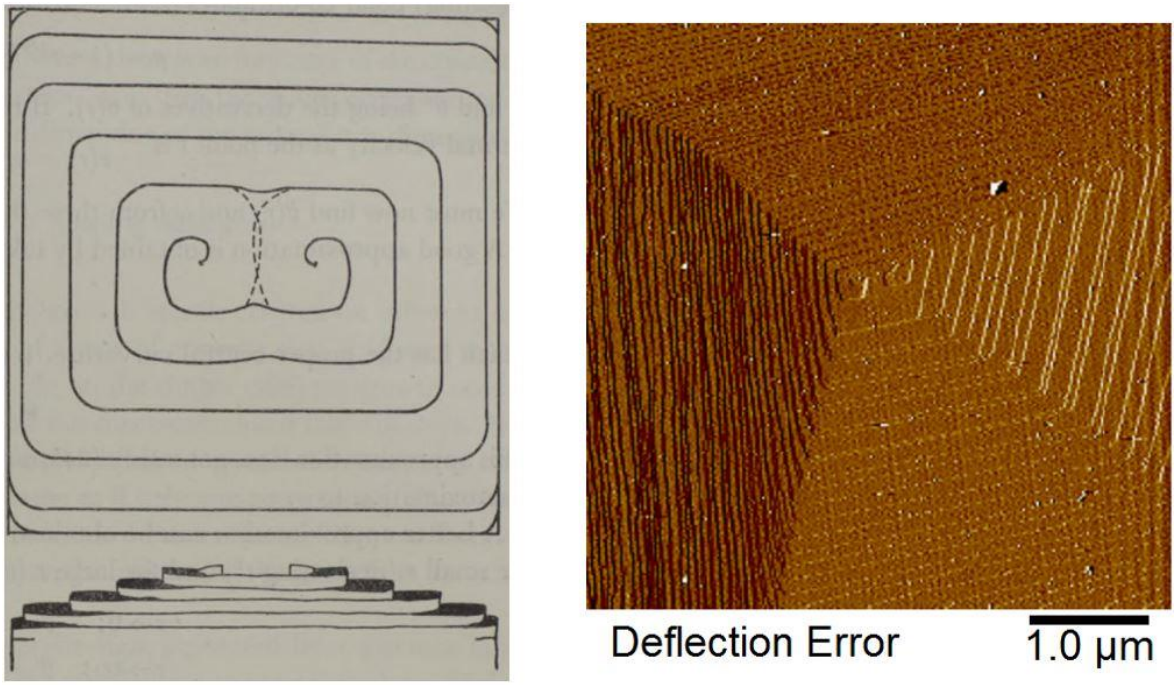

Figure 3.1. (Left) Sketch of a hillock nucleated from two dislocation sources of opposite handedness further than half a critical length apart theorized by BCF in 1951. The hillock produces concentric loops of steps. (Right) AFM data showing a calcite hillock nucleated from two dislocation sources of opposite handedness further than half a critical length apart. The AFM data corroborates the theory of BCF [2].

The results of this thesis make steps towards understanding the phenomenological link between atomic scale and bulk scale morphology in calcite. The results of this thesis also diminish the gap in knowledge between the calcite growth mechanisms on the scale of an individual hillock and on the scale of the bulk crystal. We believe that the fundamental concepts from this thesis translate well to other materials that grow via spiral growth. Understanding hillock interactions in calcite and other materials helps us understand how marine organisms are able to form biominerals, and ultimately, will aid in the pursuit of creating new and better materials through a biomimetic approach.

3.1 References

1. De Yoreo, J.J., Vekilov, P.G. Principles of Nucleation and Growth. *Reviews in Mineraleology & Geochemistry*. **54**, 57-93 (2003).

2. Burton, W.K., Cabrera, N., Frank, F.C. THE GROWTH OF CRYSTAS AND THE EQUILIBRIUM STRUCTURE OF THEIR SURFACES. *Proc. R. Soc. Lond. A*. **243**, 299-358 (1951)

3. Fu, G., Qiu, S.R., Orme, C.A., Morse, D.E., De Yoreo, J.J. Acceleration of calcite kinetics by abalone nacre proteins. *Lawrence Livermore National Laboratory*. (2005).

4. Raiteri, P., Gale, J.D., Quigley, D., Rodger, P.M. Derivation of an Accurate Force-Field for Simulating the Growth of Calcium Carbonate from Aqueous Solution: A New Model for the Calcite-Water Interface. *J. Phys. Chem. C.* **114**, 5997-6010 (2010).

5. De La Pierre, M., Raiteri, P., Gale, J.D. Structure and Dynamics of Water at Step Edges on the Calcite $\{10\bar{1}4\}$ Surface. *Cryst. Growth*. **16**, 5907-5914 (2016).